Proceedings of the 25th International Conference on
Port and Ocean Engineering under Arctic Conditions
June 9-13, 2019, Delft, The Netherlands

Bulk constitutive law and its importance in CEM simulations of ice-structure interaction

Jin Zhang[1], Dianshi Feng[1], Sze Dai Pang[1]
[1] Department of Civil & Environmental Engineering, National University of Singapore

ABSTRACT

Sea ice is often considered as quasi-brittle material which fractures and the cohesive element method (CEM) has seen increased use in recent years for the simulation of ice-structure interactions. In this method, the ice sheet is modeled using bulk elements which are connected by zero-thickness cohesive elements. The cohesive elements are deleted once their energy to resist crack formation is fully consumed, while the bulk elements retained in the system account for crushing and progressive rubbling of the ice fragments. Although the approach is physics-based leading to better potential for acceptability, a coherent guideline for the numerical inputs is still lacking. At current, past studies for CEM implementation have mainly focused on the definition of the cohesive elements traction-separation law while the bulk constitutive law has received less attention. Therefore, this paper provides an in-depth review of the bulk constitutive law and it is found to play an important role in CEM simulations of ice-structure interaction, especially scenarios involving dominant crushing failure such as vertical structures. Various shapes of the bulk constitutive law were investigated and the softening response was been found to have profound influence on the corresponding ice-induced forces for simulations involving crushing failure of the ice sheet.

KEY WORDS: Ice-structure interaction; Cohesive element; Fracture; Bulk constitutive law.

INTRODUCTION

Growing interest in the Arctic regions and advancements in technology have been driving the development and refinement of numerical tools to supplement existing empirical predictions of ice-induced forces on offshore structures. One such numerical method is the cohesive element method (CEM) which has been widely used in other engineering areas to simulate fracture for a variety of materials, including polymers, metals, concrete, and composites etc. CEM is fundamentally based on the Cohesive Zone Method (CZM) which was pioneered by Barenblatt (1959, 1962) and Dugdale (1960) for applications in the fracture of brittle and ductile materials respectively. Crack initiation and propagation in quasi-brittle concrete was implemented in the finite element framework by Hillerborg et al. (1976) with the use of CZM which accounts for energy balance due to stress redistributions caused by the macroscopic

fracture process zone. Sea ice is also known to be a quasi-brittle material and has been observed to undergo brittle fracture with relatively little plastic deformation (Bažant, 1999). Subsequently, Mulmule and Dempsey (2000, 1997) proposed the use of CZM to describe the behavior of ice.

In recent years, there has been increased used of CEM for simulating ice-structure interactions: Gürtner et al. (2010) and (Wang et al., 2019) looked into ice action against vertical structures such as lighthouses, Daiyan and Sand (2011) simulated ice interaction with a wide sloping structure, (Liu and Wu, 2012) focused on ice interaction with truss type structures, while (Lu et al., 2014) and (Wang et al., 2018) looked at conical structures. The general use of this method involves modeling the ice sheet, as illustrated in Figure 1, with bulk elements which are inter-connected by cohesive elements. The cohesive elements do not represent any physical material but describe the tractive forces which resist the separation of adjacent bulk elements. Once their energy to resist crack formation is fully consumed, the cohesive elements are deleted while the bulk elements are retained in the system account for crushing and progressive rubbling of the ice fragments. CEM has been known to be advantageous at being able to physically simulate the ice fracture and fragmentation process while simultaneously satisfying conservation laws. However, a deeper review of the various adoptions by the different researchers shows that a unified approach for the selection of numerical inputs is still lacking and no coherent guideline has been developed yet.

(a) Bulk elements displayed   (b) Cohesive elements displayed   (c) Sharing of nodes between bulk and cohesive
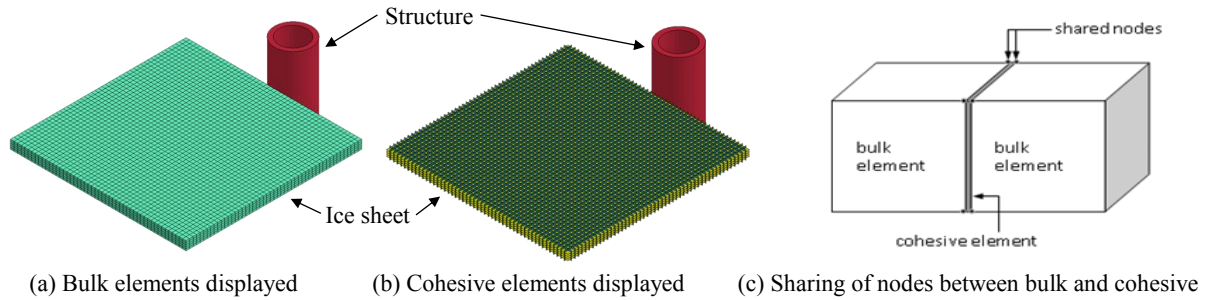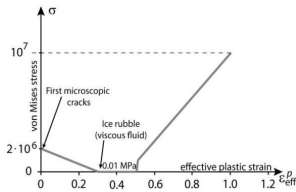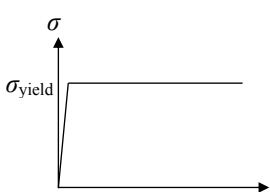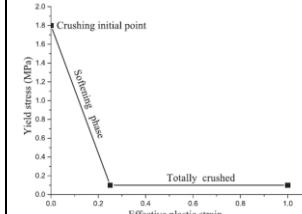
Figure 1: The ice sheet is discretized into bulk elements which are connected by zero-thickness cohesive elements

REVIEW OF EXISTING CEM IMPLEMENTATION

Past studies involving CEM implementation for ice-structure interaction have mainly focused on the definition of the cohesive elements' traction-separation law while the bulk constitutive law has received much less attention. Table 1 summarizes material input parameters for various studies and it can be quickly observed across the cases that the cohesive input parameter fracture energy G_c varies by almost three orders of magnitude while the bulk elements take on vastly different constitutive relationships: some cases employ linear plasticity while others implement assumed softening. Most literature focused on the discussion and definition of the cohesive parameters while less studies have detailed the motivation for the bulk input parameters. Therefore, this paper examines the bulk constitutive law deeper while following the approach in which the cohesive elements play a more dominant role in the macroscopic fracture processes such as the radial and circumferential cracks while the bulk elements are responsible for the microscopic fragmentation processes within the large ice floes (Feng et al., 2018). In order to investigate the effects of various aspects of the bulk constitutive law on the ice-structure interaction forces, sensitivity studies were performed and the results are presented in the next section.

Table 1: CEM material properties used for various simulations of ice-structure interactions.

Various papers	Gürtner et al. (2010) Numerical modelling of a full scale ice event	Lu et al. (2014) Simulating ice-sloping structure interactions with the cohesive element method	Wang et al. (2018) A simulation study on the interaction between sloping marine structure and level ice based on cohesive element model
Structure width (m)	7.52	13.6	13.6
Ice sheet (m)	40 x 40 x 0.69	50 x 50 x 0.33	55 x 55 x 0.33
Element type & size l x l x t (m)	Hexahedral 0.2 x 0.2 x 0.13	Regular tri-prism 0.625 x 0.625 x 0.33	Regular tri-prism (0.25~1) x (0.25~1) x 0.33
Cohesive element properties TSL shape	T_{max} (vertical) = 1.0 MPa T_{max} (horizontal) = 1.1 MPa **G_c = 5200 J/m^2** Trapezoidal TSL	T_{max} = 0.539 MPa **G_c = 15 J/m^2** Bilinear TSL	T_{max} = 0.8 MPa S_{max} = 0.9 MPa G_c = 30 J/m^2 Bilinear TSL
Bulk element properties	E = 5 GPa σ_{yield} = 2 MPa v = 0.3 **Softening elastoplastic with hardening** 	E = 0.35 GPa σ_{yield} = 1 MPa ρ = 909 kg/m^3 **Elastic, perfect-plastic** 	E = 5 GPa σ_{yield} = 1.8 MPa v = 0.3 ρ = 910 kg/m^3 **Softening elastoplastic failure strain**

SENSITIVITY STUDY

The sensitivity studies were performed using a CEM model of level ice sheet interacting with a vertical structure as shown in Figure 2(a). The ice crushing failure process in this problem is expected to be predominantly governed by the constitutive behavior of the bulk elements. The ice sheet has a dimension of 20 m x 20 m x 1 m with mesh size $l_{ele} \approx 0.3$, while the cylindrical structure has a diameter of 3.2 m. In the simulations, the rigid cylindrical structure was moved towards the ice sheet at a constant velocity of 0.5 m/s – a rate at which brittle crushing is expected – while nodes at the perimeter of the ice sheet excluding the incident edge were held laterally in place. Zero-thickness cohesive elements are inserted between bulk elements which form the ice sheet. The numerical parameters for the cohesive elements were kept constant for all cases with G_c = 15 J/m^2 as shown in Figure 2(b).
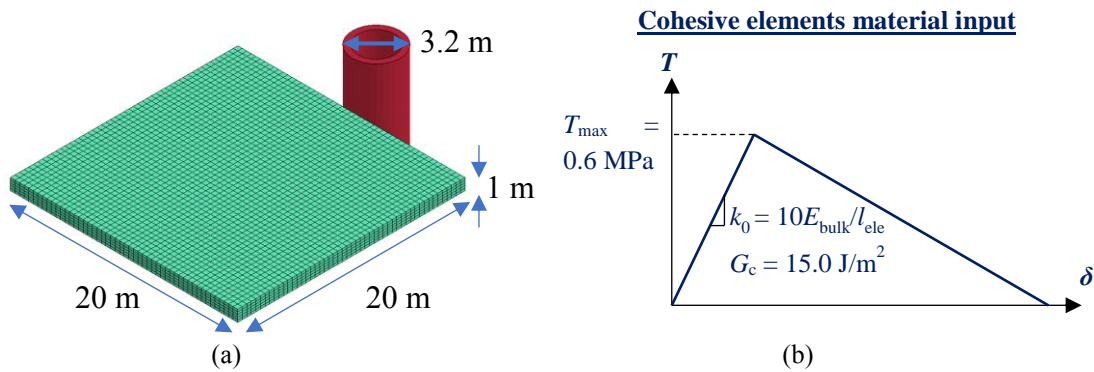

Figure 2: (a) CEM model for crushing interaction and (b) corresponding TSL input for cohesive elements.

General Shape

A few general shapes for the bulk constitutive law as illustrated in Figure 3 were investigated. The simplest shape considered in this study was the purely elastic case with Young's modulus $E = 3.5$ GPa, while the elastic-plastic case had a yield criterion of 3.3 MPa and the stress remained constant during the plastic phase till a failure strain of 1.0, after which the bulk element was eroded because excessively distorted elements would have slowed down the computations significantly. It is reasonable to remove these elements because in reality they represent pulverized ice which should no longer have significant contribution to the ice-induced forces generated on the structure. The failure strain of 1.0 was adopted for all cases considered here and set in accordance with previous CEM studies of ice-structure interactions.

The elastic-softening case takes its shape from the stress-strain curve shown in Figure 4(a) which was obtained from physical compression test of sea ice by Richter-Menge (1992). The initial slope is the Young's modulus E while the yield stress is denoted by σ_y. The curve has a post-peak softening response and the area under the curve is defined as the plastic dissipation energy. The plot from Richter-Menge (1992) was digitized and curve-fitted to obtain the mathematical equation that describes the shape of the softening phase. Nevertheless, the softening response at high strains have seldom been reported in literature. In the example shown in Figure 4(a), the stress-strain curve was only reported by the author up to a strain of 5%. Hence, for the sake of simplicity, a perfectly-plastic response was assumed between the final available value and the failure strain of 1.0. Similar to other cases shown in Figure 3, the values for E and σ_y were set at 3.5 GPa and 3.3 MPa respectively.

Finally, the elastic-softening-hardening case based on the shape proposed by Gürtner et al. (2010) which is reproduced in Figure 4(b) was also investigated for comparison. Using the information from Gürtner et al. (2010) and (Hilding et al., 2012, 2011), the elastic-softening-hardening shape was modified to match the Young's modulus of 3.5 GPa and yield stress of 3.3 MPa which were standardized throughout this sensitivity study, followed by linear softening up to a strain of around 0.3. A perfectly-plastic phase with plateau stress of 0.01 MPa was imposed between strain values of 0.3 and 0.5, and thereafter a linear hardening phase with initial gradient of 100 MPa followed by a gentler gradient of 20 MPa.
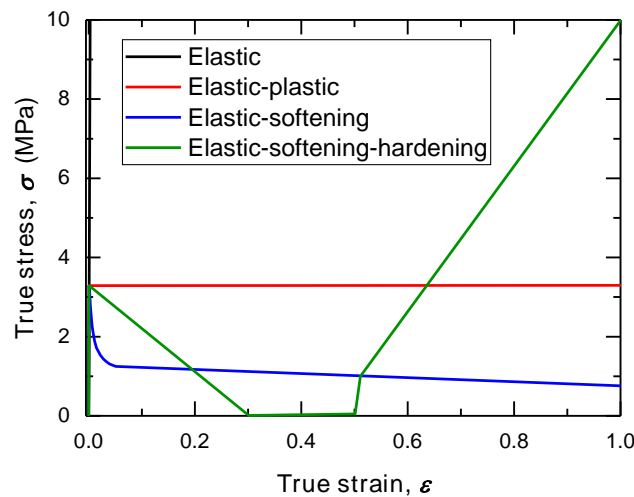

Figure 3: Constitutive stress-strain laws with various generic shapes.

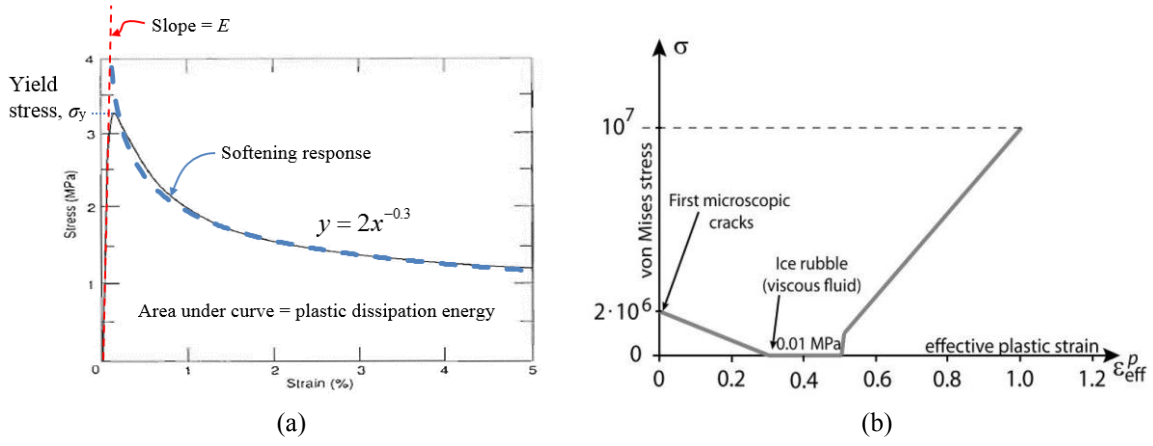(a)   (b)

Figure 4: (a) Stress-strain result from physical compression test of Antarctic sea ice by Richter-Menge (1992) with curve-fitted equation for softening response, and (b) Von Mises stress vs effective plastic strain adopted for homogenized CEM model by Gürtner et al. (2010), Hilding et al. (2011), and Hilding et al. (2012).

Snapshots of the CEM simulation at various time instances are shown in Figure 5 to highlight the interaction process. There is an initialization phase of around 2 seconds before the initial interaction between the ice sheet and the structure. Interaction contact gradually increases until full width of the cylinder is achieved at $t = 6$ s, after which there is continuous crushing. The resulting ice-induced force-time histories obtained for the ice-structure interaction are plotted in Figure 6, together with the mean forces during the continuous crushing phase and corresponding standard deviations.

$t = \sim 2$ s $t = 6$ s $t > 6$ s
Initial interaction   Onset of continuous crushing   Continuous crushing phase
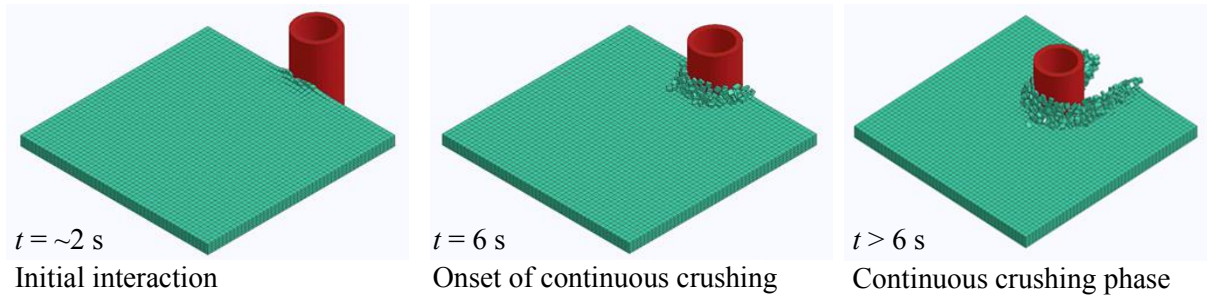
Figure 5: Snapshots of simulation at various time instances to highlight interaction process.
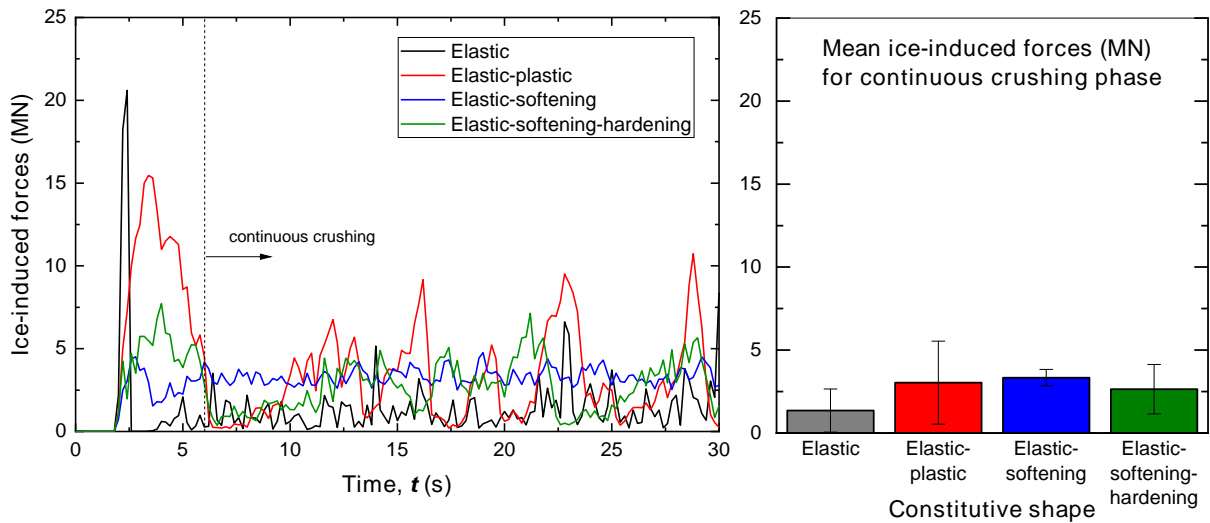

Figure 6: Force-time history and mean ice-induced forces for cases with different bulk constitutive laws.

From the force-time histories in Figure 6, it can be observed that the elastic case has the highest initial peak load but thereafter the lowest continuous crushing force. Slightly more explosive fragmentation was seen in this case as compared to the other cases. The higher initial load is expected since the bulk elements do not yield and the load builds up until the cohesive elements start to fail. Once the crushing failure process has been set in motion, the bulk elements quickly unload their stored elastic energy onto adjacent cohesive elements, causing them to fail rapidly resulting in a low mean force.

While the elastic case demonstrates rapid buildup of energy with explosive disintegration, the elastic-plastic case has a perfectly-plastic region in the bulk constitutive law which caps the rate of energy buildup. Thus, the load is able to increase in a more stable manner before the cohesive elements begin to fail, resulting in cyclic loading with peak forces of almost 10 MN but with higher amplitude i.e. larger standard deviation. In contrast, the elastic-softening case has the most stable mean force with a standard deviation of less than 0.5 MN but also the highest mean force compared to the other cases.

From these results, it can be seen that the shape of the bulk constitutive relationship has considerable influence on the predicted ice-structure interaction forces and hence is an important parameter. The elastic-softening stress-strain law is more commonly observed in compression tests on ice and was used for the rest of the sensitivity study.

Yield Stress

To investigate the sensitivity of the ice-induced forces towards the yield stress, two sets of studies were performed: (a) varying the yield stress with a fixed failure strain, and (b) varying the yield stress while maintaining the softening rate of the stress-strain curve. The plastic dissipation energy, i.e. area under the curve, used in these two sets of studies was kept constant. In this first set of cases with *fixed failure strain*, the Young's modulus E of 3.5 GPa and effective plastic strain limit $\varepsilon_{p,fail}$ of 1.0 were kept constant for all cases while modifying the yield stress σ_y. This was achieved by translating the softening curve from Figure 4(a) horizontally and truncating the vertical peak of the curve when it coincides with the elastic slope. The corresponding stress-strain curves with varying post-peak softening rates are shown in Figure 7. The resulting force-time histories, mean values and standard deviations of the ice-induced forces are shown in Figure 8. Apart from the differences in the initial peak loads, the continuous crushing phase (after $t = 6$ s) is observed to have similar characteristics and the mean ice-induced forces are fairly constant for the range of yield stress investigated.
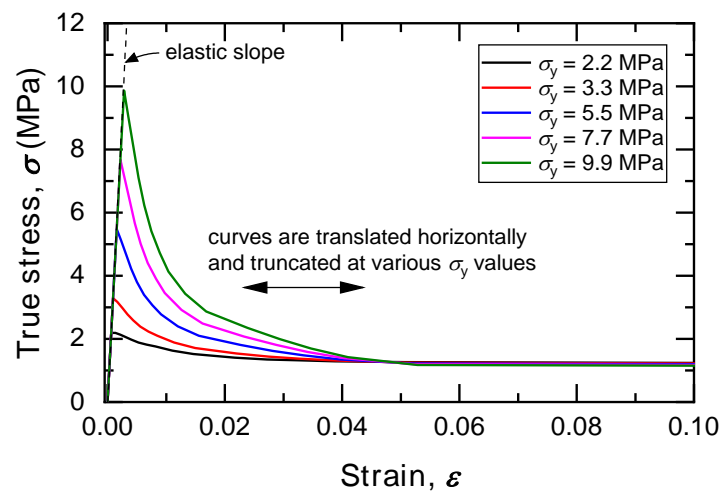

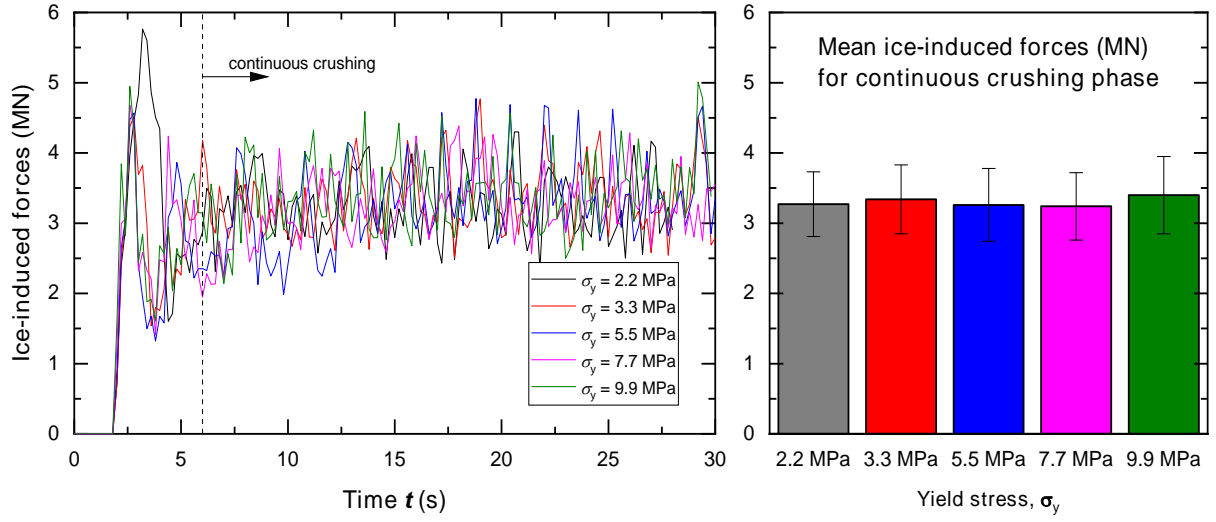Figure 7: Bulk constitutive laws with varying yield stress but fixed failure strain ($\varepsilon_{p,fail} = 1.0$).

Figure 8: Force-time history and mean ice-induced forces for bulk constitutive laws with varying yield stress σ_y but fixed failure strain ($\varepsilon_{p,fail} = 1.0$).

In the second set of cases with *fixed softening rate*, the Young's modulus E was fixed at 3.5 GPa but the yield stress σ_y was varied by fixing the post-peak softening rate of the curve while translating it vertically according to the set yield stress values. To maintain the same amount of energy for each curve, the area under each curve was kept constant by varying the effective plastic failure strain $\varepsilon_{p,fail}$ (i.e. the curves with higher yield stress will be truncated at a smaller effective plastic failure strain). The corresponding stress-strain curves are illustrated in Figure 9. The resulting force-time histories, mean values and standard deviations of the ice-induced forces are shown in Figure 10. For this set of results, it is apparent that the mean value of the ice-induced forces and its standard deviation rise proportionally with the increase in the yield stress. The data points have a good linear fit with an R^2 value of 0.99 when subsequently plotted in Figure 11.
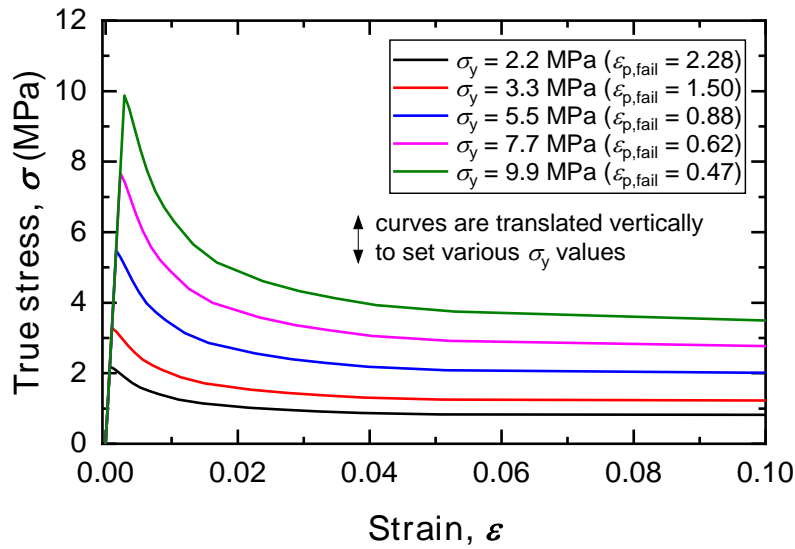

Figure 9: Bulk constitutive laws with varying yield stress but fixed energy and softening rate.
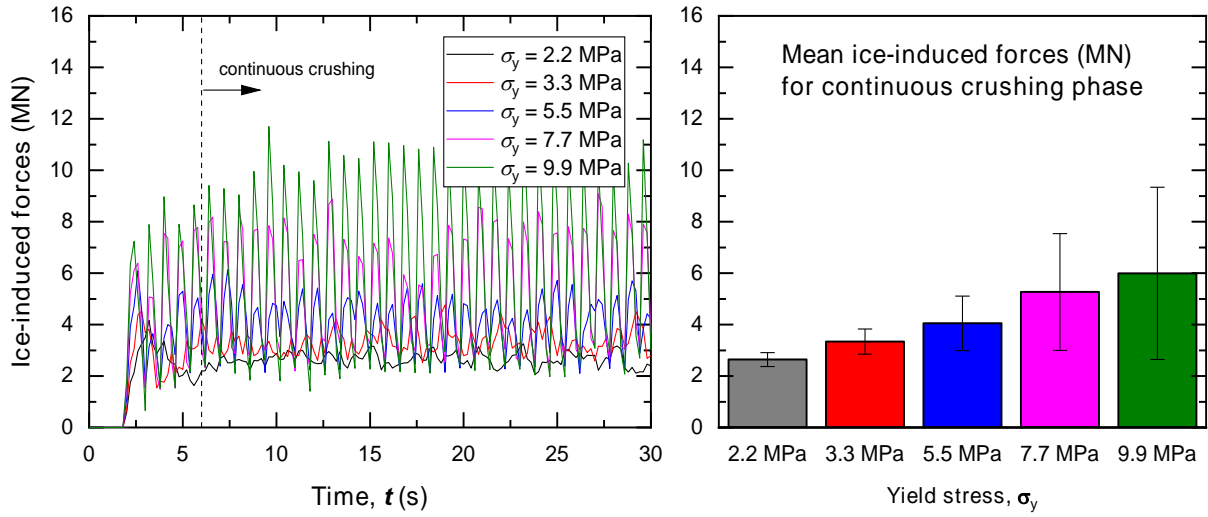
Figure 10: Force-time history and mean ice-induced forces for bulk constitutive laws with varying yield stress σ_y but fixed energy and softening rate.

Figure 11 also compares both sets of results where the stress-strain curves were adjusted using the two approaches. With energy (the area under stress-strain curve) fixed, varying the yield stress while keeping the failure strain fixed has minimal effect on the mean ice-induced force. This is probably because the post-peak strength of the material does not vary significantly for these cases as shown in Figure 7 while only the initial part of the stress-strain curve was varied. On the other hand, when the shape of the curve was fixed and failure strain was reduced while increasing the yield stress to maintain the same energy, the mean ice-induced force increases linearly with the yield stress. This may be due to the higher post-peak strength of the material as shown in Figure 9. Also, it can be observed that the resultant ice force is larger when the plastic dissipation energy is concentrated within a region of lower strain in the stress-strain curve.
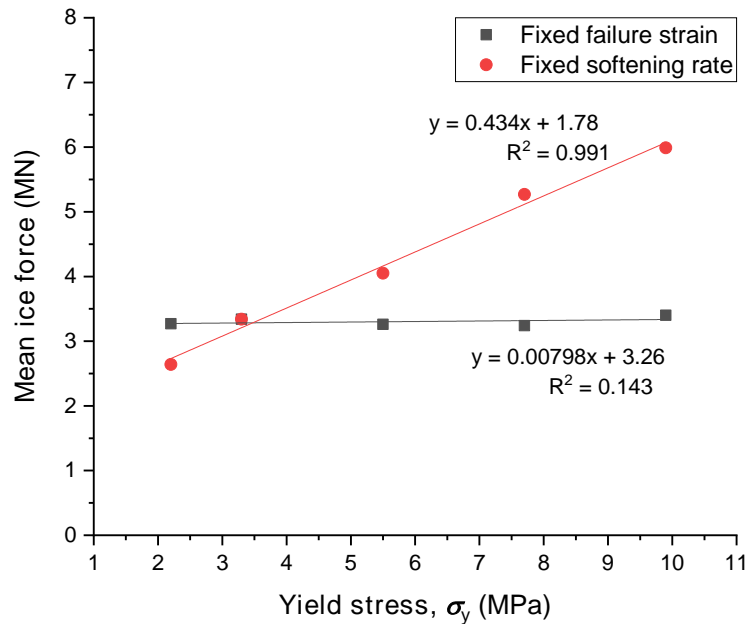

Figure 11: Comparison of sensitivity towards varying yield stress with (a) fixed failure strain and (b) fixed softening rate of the bulk stress-strain curve.

Rate of Softening

The effect of the rate of softening in the bulk constitutive law is further examined in this section. Figure 12 shows various stress-strain curves with different softening rates after the immediate post-peak drop in stress. The plastic dissipation energy was not kept constant for these cases. The resulting force-time histories, mean values and standard deviations of the ice-induced forces are shown in Figure 13. It can be observed that the softening phase of the stress-strain law has significant impact on the predicted ice-induced forces. As the rate of softening increases, i.e. softening phase becomes steeper and hence the plastic dissipation energy is reduced, the mean value of the ice-induced force drops.
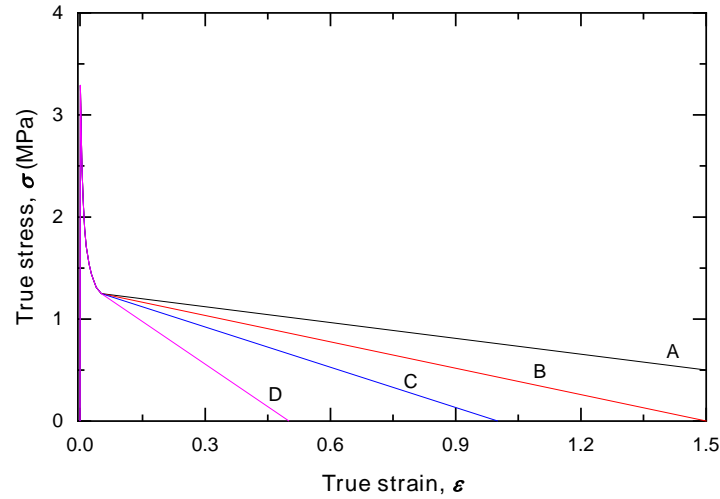
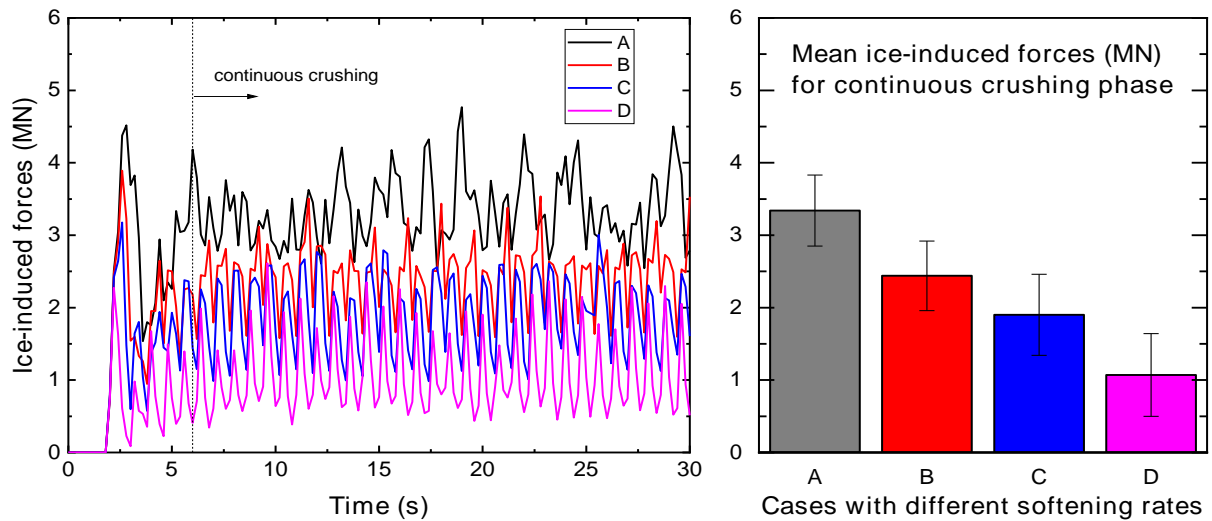Figure 12: Bulk constitutive laws with different softening rates.

Figure 13: Force-time history and mean ice-induced forces for bulk constitutive laws with different softening rates.

EXPERIMENTAL CALIBRATION OF POST-PEAK RESPONSE

As seen above, the shape of the bulk constitutive law has considerable influence on predicted ice-induced forces in ice-structure interactions. The simulation results are highly sensitive to the yield stress and softening parameters. It is therefore extremely important to properly define the bulk constitutive law in order to accurately capture the ice-induced forces. The sound

physics-based step forward would be to make use of physical compression test results for the calibration of the stress-strain input.

Many researchers have investigated uniaxial compression of ice samples, examining the effects of strain rate, temperature, brine volume, etc. Besides uniaxial compression tests, some researchers have also studied the compression of ice under triaxial loading (Cox and Richter-Menge, 1985; Gratz and Schulson, 1997; Kalifa et al., 1992; Melanson et al., 1999) and compared their results to those from unconfined uniaxial compression tests. Figure 14(a) illustrates an unconfined uniaxial compression test while Figure 14(b) presents the schematic diagram of a triaxial compression test.

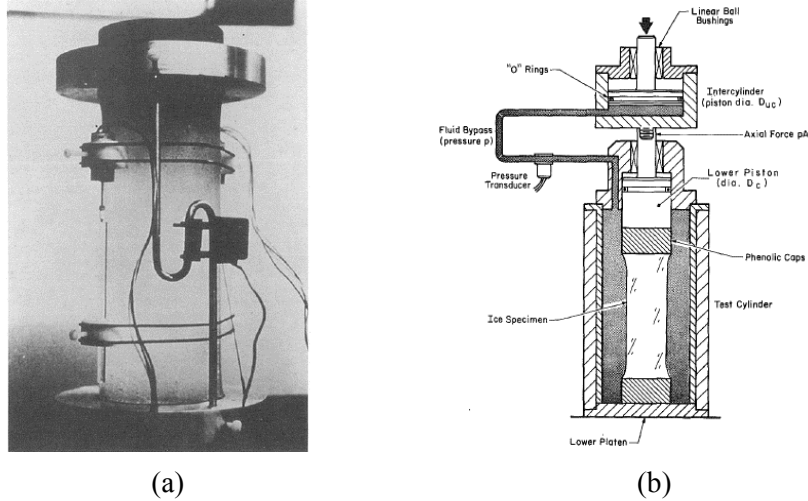(a)   (b)

Figure 14: (a) Unconfined uniaxial compression test and (b) Schematic diagram of triaxial compression test (Richter-Menge, 1991).

Nevertheless, the majority of physical stress-strain data has been obtained through uniaxial compression tests of ice core samples. Because of the brittleness of the ice, the post-peak softening was rarely captured due to the explosive fragmentation when the specimens disintegrated. However, in ice-structure interactions where crushing is involved, the stress state of the ice is rarely unconfined. As an ice sheet loads on a structure, it is laterally restrained but is allowed to displace in the vertical direction. The level ice sheet can be considered as a plate with minimal restraint in the out-of-plane direction (only buoyancy and gravitational forces act along the vertical axis). Hence, the ice within the crushing zone during an ice-structure interaction typically experiences confinement as illustrated in Figure 15. In the simplest form of thin ice, the confinement tends towards a biaxial stress state.
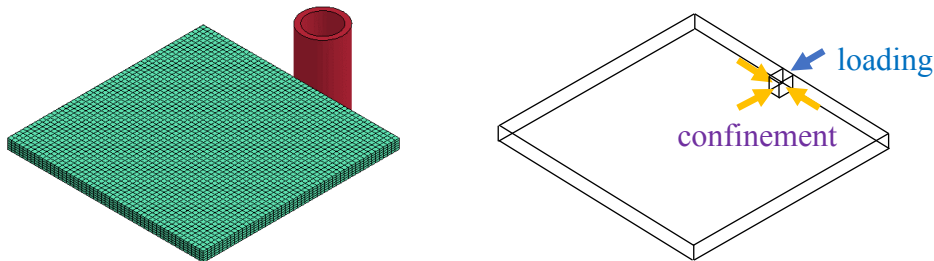

Figure 15: Illustration of confinement in an ice sheet during loading.

Therefore, the constitutive law for the bulk elements in a CEM model of ice-structure interaction problem could be more accurately captured using biaxial strength parameters. The biaxial stress state of ice has been investigated in the past for both fresh water ice and sea water ice. Smith and Schulson (1993) and Iliescu and Schulson (2004) studied the brittle compressive failure of fresh water columnar ice under biaxial loading, while Smith and Schulson (1994)

looked into that of salt water columnar ice. Schulson and Buck (1995) examined the ductile to brittle transition of orthotropic fresh water columnar ice under biaxial compression and found the ductile failure envelopes. In similar manner, Schulson and Nickolayev (1995) studied the biaxial loading of saline ice at various strain rates. The peak stress values were used to derive the failure envelopes. However, the softening phase is mostly missing in these published results.

Thus, compression tests on ice in the literature have commonly been focused on peak values only while stress-strain data have often been terminated shortly after brittle failure. There is lack of experimental data on the softening phase of the stress-strain curve under brittle crushing at large deformation. This phase is particularly important for the material input of the bulk elements in the CEM model since it is supposed to account for microscopic cracking in the elements. Therefore, to obtain data on this softening phase a confined compression test was designed and carried out in this study. It is expected that the confinement will contribute to volumetric retention after the initial failure at peak load (due to splitting/spalling), allowing for further crushing of the broken ice fragments into granular form. The secondary fracture phase would be accounted for by the extended stress-strain measurements.

PILOT STUDY SHOWING IMPORTANT CONSIDERATION OF CONFINEMENT

Due to limitations in the testing facilities, only a pilot test was carried out in this study as a proof of concept. Ice cube specimens were prepared by freezing fresh water in PVC moulds from temperature of +25°C down to -10°C over 20 hours. Insulation on the sides and base of the moulds promoted top-down freezing which is observed in nature. Confined-compression tests were carried out in an air-conditioned cool environment using the setup shown in Figure 16. For each test, the ice specimen was placed between lateral confinement plates which were secured in position by steel confinement rods. To minimize heat transfer, the confinement plates were constructed using acrylic sheets which have relatively low thermal conductivity, and prior to the compression test the confinement rig was thermally conditioned in a freezer to a temperature of -10°C. The specimens were compressed at a rate of 1 mm/s which was roughly equivalent to a strain rate of 10^{-2} s^{-1} at which brittle fracture is expected to occur. Loading was terminated when the crushed ice fragments displacing in the unconfined direction began to press against the confinement rods. The tests were stopped when this condition occurred in order to prevent the confinement rods from interfering with the load-displacement results.
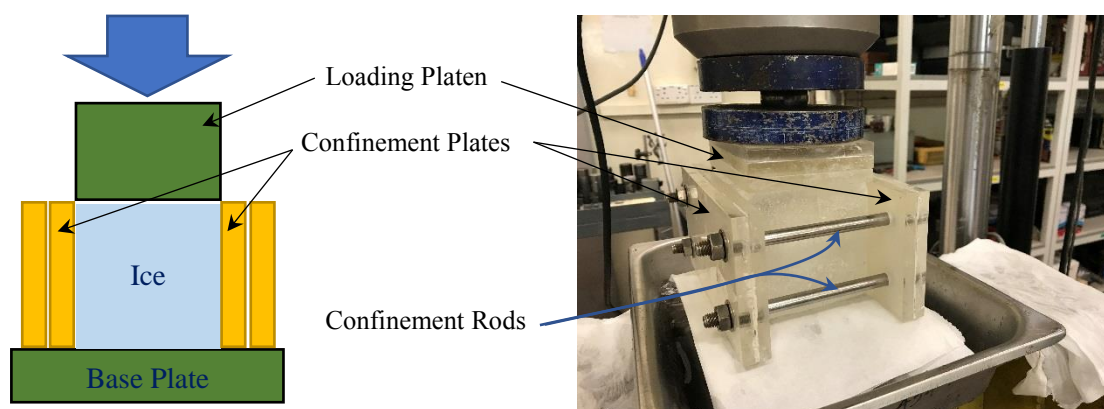

Figure 16: Confined compression test setup.

Figure 17(a) shows the end state at which the crushed ice was almost touching the confinement rods. With the confinement plates removed as shown in Figure 17(b), the crushed ice fragments were observed to have a granular size of around 1 mm to 2 mm, which is similar to the previous observations by Palmer and Sanderson (1991) and Tuhkuri (1994).

Figure 17: (a) Crushed ice under lateral confinement and (b) view of granular ice fragments with confinement platens removed.

A Yokogawa digital oscilloscope was utilized to record the load-displacement data from the tests. The resulting stress-strain curves for six specimens are shown in Figure 18. The apparent Young's modulus is around 0.4 GPa which is one order of magnitude lower than that commonly reported in the literature. This error could be due to sample preparation where the ends were not precisely flat and sanded down, which was a limitation of the molds used to prepare the specimens. Another reason could be the lack of initial preloading before the tests commenced. However, the more important aspect of the test results is the overall shape of the stress-strain curves when the specimens were subjected to large deformation. The strains achieved in this test were up to 0.13 while those in existing published literature have been mostly up to 0.0015. The post-peak softening rate is about one-third of the Young's modulus, followed by a plateau stage with stress magnitude of about 25% of the peak stress. Moreover, some hardening occurs after an effective plastic strain of 0.08. Nevertheless, it is recognized that specimen preparation is highly important, and less than ideal conditions can lead to large variations in test results. Therefore, it is maintained that only preliminary observations can be made from the pilot test in this thesis. Proper facilities and equipment with extensive testing will be required to obtain reliable stress-strain inputs.
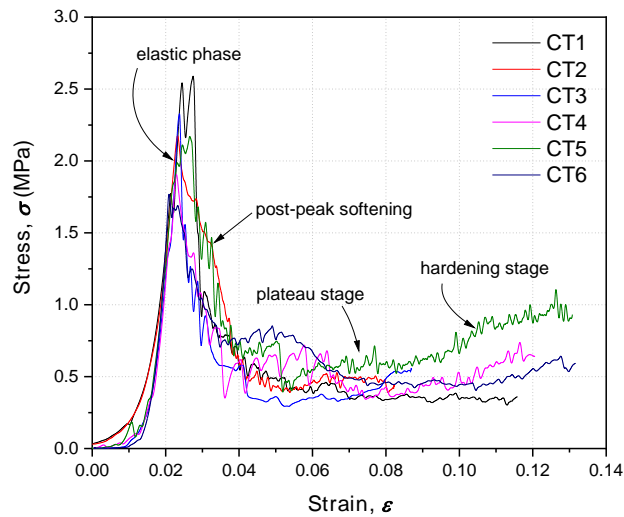

Figure 18: Stress-strain results from confined compression tests of ice cube samples.

CONCLUSIONS

An in-depth review of the bulk constitutive law was carried out in this paper. The overall shape of the bulk constitutive law was found to have considerable influence on predicted ice-induced

forces in ice-structure interactions, especially for dominant crushing failure scenarios such as ice interaction with vertical structures. The simulation results were found to be sensitive to the yield stress but more dominantly controlled by the softening parameters. It is therefore extremely important to properly define the post yield aspect of the bulk constitutive law in order to accurately predict the ice-induced forces. Unfortunately, majority of the available physical compression test results are based on uniaxial testing which is unable to capture the post yield softening effects and therefore does not accurately reflect the micro intergranular cracking occurring during crushing. In the simplest form of thin ice sheet interacting with a vertical structure, the confinement tends towards a biaxial stress state. Therefore an equivalent confined compression test was designed and proposed in this paper. Preliminary observations from the pilot test study showed substantial plateau stage after the initial post-peak softening. Further refinement in the test equipment and procedure will be required to obtain reliable stress-strain inputs which can then be implemented in a material model that takes care of various states of confinement, crucial to the accurate capture of the crushing behavior of ice.

ACKNOWLEDGEMENTS

REFERENCES

Barenblatt, G.I., 1962. The Mathematical Theory of Equilibrium Cracks in Brittle Fracture. *Advances in Applied Mechanics*, 7, 55–129.

Barenblatt, G.I., 1959. The formation of equilibrium cracks during brittle fracture. General ideas and hypotheses. Axially-symmetric cracks. *Journal of Applied Mathematics and Mechanics*, 23(3), 622–636.

Bažant, Z.P., 1999. Size effect on structural strength: A review. *Archive of Applied Mechanics*, 69(9–10), 703–725.

Cox, G.F.N., Richter-Menge, J.A., 1985. Triaxial compression testing of ice, in: *Civil Engineering in the Arctic Offshore*. ASCE, pp. 476–488.

Daiyan, H., Sand, B., 2011. Numerical Simulation of the Ice-Structure Interaction in LS-DYNA, in: *8th European LS-DYNA Users Conference*. Strasbourg.

Dugdale, D.S., 1960. Yielding of steel sheets containing slits. *Journal of the Mechanics and Physics of Solids*, 8(2), 100–104.

Feng, D., Zhang, J., Yap, K.T., Pang, S.D., 2018. Influence of Cohesive Stiffness on Cohesive Element Method Based Simulation of Ice-Structure Interaction, in: *24th IAHR International Symposium on Ice*. Vladivostok, Russia.

Gratz, E.T., Schulson, E.M., 1997. Brittle failure of columnar saline ice under triaxial compression. *Journal of Geophysical Research: Solid Earth*, 102(B3), 5091–5107.

Gürtner, A., Bjerkås, M., Forsberg, J., Hilding, D., 2010. Numerical modelling of a full scale ice event, in: *20th IAHR International Symposium on Ice*. Lahti, Finland.

Hilding, D., Forsberg, J., Gurtner, A., 2012. Simulation of loads from drifting ice sheets on offshore structures, in: *12th International LS-DYNA Users Conference*. pp. 1–8.

Hilding, D., Forsberg, J., Gürtner, A., 2011. Simulation of ice action loads on offshore structures, in: *8th European LS-DYNA Users Conference, Strasbourg, France*. pp. 1–12.

Hillerborg, A., Modéer, M., Petersson, P.E., 1976. Analysis of crack formation and crack growth in concrete by means of fracture mechanics and finite elements. *Cement and Concrete Research,*.

Iliescu, D., Schulson, E.M., 2004. The brittle compressive failure of fresh-water columnar ice loaded biaxially. *Acta Materialia*, 52(20), 5723–5735.

Kalifa, P., Ouillon, G., Duval, P., 1992. Microcracking and the failure of polycrystalline ice under triaxial compression. *Journal of Glaciology*, 38(128), 65–76.

Liu, M.L., Wu, J.F., 2012. Numerical Simulation for Ice-Truss Offshore Structure Interactions With Cohesive Zone Model, in: *IAHR 21st Intl. Symposium on Ice, Dalian University of Technology, Dalian, China*. pp. 814–825.

Lu, W., Lubbad, R., Løset, S., 2014. Simulating ice-sloping structure interactions with the cohesive element method. *Journal of Offshore Mechanics and Arctic Engineering*, 136(3), 31501.

Melanson, P.M., Meglis, I.L., Jordaan, I.J., Stone, B.M., 1999. Microstructural change in ice: I. Constant-deformation-rate tests under triaxial stress conditions. *Journal of Glaciology*, 45(151), 417–422.

Mulmule, S. V., Dempsey, J.P., 2000. LEFM size requirements for the fracture testing of sea ice. *International Journal of Fracture,*.

Mulmule, S. V, Dempsey, J.P., 1997. Stress-separation curves for saline ice using fictitious crack model. *Journal of engineering mechanics*, 123(8), 870–877.

Palmer, A.C., Sanderson, T.J.O., 1991. Fractal crushing of ice and brittle solids. *Proc. R. Soc. Lond. A*, 433(1889), 469–477.

Richter-Menge, J.A., 1992. Compressive strength of frazil sea ice, in: *Proceedings of the International Association of Hydraulic Engineering and Research Symposium on Ice*. pp. 15–19.

Schulson, E.M., Buck, S.E., 1995. The ductile-to-brittle transition and ductile failure envelopes of orthotropic ice under biaxial compression. *Acta Metallurgica et Materialia*, 43(10), 3661–3668.

Schulson, E.M., Nickolayev, O.Y., 1995. Failure of columnar saline ice under biaxial compression: Failure envelopes and the brittle-to-ductile transition. *Journal of Geophysical Research: Solid Earth*, 100(B11), 22383–22400.

Smith, T.R., Schulson, E.M., 1994. Brittle compressive failure of salt-water columnar ice under biaxial loading. *Journal of Glaciology*, 40(135), 265–276.

Smith, T.R., Schulson, E.M., 1993. The brittle compressive failure of fresh-water columnar ice under biaxial loading. *Acta metallurgica et materialia*, 41(1), 153–163.

Tuhkuri, J., 1994. Analysis of ice fragmentation process from measured particle size distributions of crushed ice. *Cold Regions Science and Technology*, 23(1), 69–82.

Wang, F., Zou, Z.-J., Zhou, L., Ren, Y.-Z., Wang, S.-Q., 2018. A simulation study on the interaction between sloping marine structure and level ice based on cohesive element model. *Cold Regions Science and Technology*, 149, 1–15.

Wang, Y., Zou, Z.-J., Wang, F., Shi, C., Luo, Y., Lu, T.-C., 2019. A simulation study on the ice fracture behaviors in ice-lighthouse interaction considering initial defects in ice sheet. *Ocean Engineering*, 173, 433–449.